

Two-person Graph Convolutional Network for Skeleton-based Human Interaction Recognition

Zhengcen Li, Yueran Li, Linlin Tang, Tong Zhang, Jingyong Su

Abstract—Graph Convolutional Network (GCN) outperforms previous methods in the skeleton-based human action recognition area, including human-human interaction recognition task. However, when dealing with interaction sequences, current GCN-based methods simply split the two-person skeleton into two discrete sequences and perform graph convolution separately in the manner of single-person action classification. Such operation ignores rich interactive information and hinders effective spatial relationship modeling for semantic pattern learning. To overcome the above shortcoming, we introduce a novel unified two-person graph representing spatial interaction correlations between joints. Also, a properly designed graph labeling strategy is proposed to let our GCN model learn discriminant spatial-temporal interactive features. Experiments show accuracy improvements in both interactions and individual actions when utilizing the proposed two-person graph topology. Finally, we propose a Two-person Graph Convolutional Network (2P-GCN). The proposed 2P-GCN achieves state-of-the-art results on four benchmarks of three interaction datasets, SBU, NTU-RGB+D, and NTU-RGB+D 120.

Index Terms—Skeleton-based interaction recognition, action recognition, graph convolutional networks, skeleton topology

I. INTRODUCTION

Human-human interaction recognition becomes increasingly important, which aims at identifying mutual activities from videos and mainly benefits content-based retrieval, security and surveillance, and human-robot interaction [1]. Conventional methods for activity detection and recognition from videos consist of video processing techniques and machine learning approaches.

Skeleton capturing devices [2] and pose estimation algorithms [3], [4] provide economical approaches to obtaining accurate body key-point coordinates. Compared with regular RGB videos, representing the human body as a set of key points (skeleton joints) in 3D space shows more robustness against obstruction and requires less computation. Therefore, many researchers have put their efforts into skeleton-based action recognition [5]–[10].

Theoretically, it is more challenging to semantically analyze and technically identifying human interactions than single-person actions [11]. Despite significant progress in regular action recognition, it remains hard to extract multi-person skeleton data from videos and recognize the interactions [12]. This

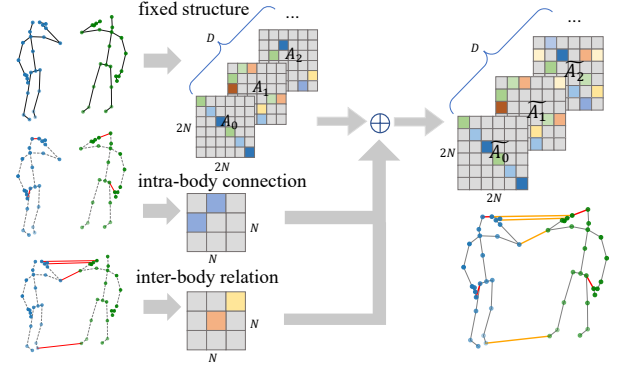


Fig. 1. Illustration of the construction of the proposed two-person graph. N is the number of joints in each person, and D is the maximum graph sampling distance.

work focuses on a simple yet essential landmark, skeleton-based two-person interaction recognition.

Existing interaction recognition approaches can be categorized into hand-crafted models and deep learning approaches. Traditional methods [5], [13]–[15] mostly start with specified prior knowledge and introduce typical feature representations, then use a classifier like SVM to group transformed vectors. More recent solutions [10], [16]–[18] utilize CNN or RNN to extract information from joint coordinates, motion patterns or features processed by hand-crafted techniques. These models cannot directly process non-Euclidean skeleton data. Therefore, they often need specific processing for target datasets to achieve competitive performance.

Recently, Yan et al. [9] introduced Graph Convolution Network into skeleton-based action recognition. Numerous GCN-based works [9], [19]–[24] show the advantage of GCN in extracting spatio-temporal features from graph-structured skeleton data. Most existing work split two-person skeletons apart for interaction sequences containing two persons in each frame and consider them as two samples [9], [19], [21], [22], [24]. Finally, the two separate skeletons are fed into the single-person GCN model. Despite the improvement in conventional single-person recognition, such methods failed to model valuable interactive information. In this work, we introduce a novel two-person graph to represent interactions, as shown in Fig.1. Besides the pre-defined two separate physical skeletons, the relational adjacency matrix can depict the correlation between joints from the same person (intra-body connections far away in the physical graph) and between two persons' joints (inter-body relation). To effectively model these intra-body and inter-body connections, the graph edge

Corresponding author: Jingyong Su (e-mail: sujingyong@hit.edu.cn)

Zhengcen Li, Yueran Li, Linlin Tang and Jingyong Su are with the Harbin Institute of Technology (Shenzhen), Shenzhen 518055, China

Tong Zhang and Jingyong Su are with the Peng Cheng Laboratory, Shenzhen 518055, China

Code is available on-line at <https://github.com/mgiang/2P-GCN>

labeling strategy is introduced to decide how the edges connect between joints and their correlation strength. Finally, a refined two-person graph is constructed as a representation of two-person interactions. With this representation, GCN enables the ability to accumulate intra-body features and interactive features simultaneously.

It is worth mentioning that the two-person graph representation is compatible with the single-person scenario. A two-person graph keeps the same information as the single-person graph when remaining zeros for the second person. Furthermore, the two-person graph contains more information. For example, to reflect individual actions which are a part of interactions (e.g., making phone calls), we can create a mirror skeleton as an imagined second person; to depict human-object interactions more precisely, we can introduce additional key-points to stand for objects. In our ablation experiments, our two-person graph representation also improve the accuracy of individual actions.

Based on the two-person graph, we then introduce Spatial Graph Convolution (SGC) and Temporal Convolution (TCN), which form a basic block of the GCN network. To verify the effectiveness of the two-person graph representation, we apply the two-person graph convolution in several GCNs and find that our two-person graph representation can significantly improve their performance in recognizing interactions. Finally, we extend ResGCN [21] with our two-person convolution block. Experiments conducted on three public interaction action datasets [5], [7], [25] show that our model outperforms existing approaches.

Our main contributions can be summarized as follows.

- We introduce the two-person graph representation as a substitution for the separated skeleton graph. Compared with the isolated single-person graph structure, our two-person graph unifies the notation of the inter-body correlations and intra-body correlations.
- Based on the two-person graph, a series of graph edge labeling strategies are designed to depict the joint correlation beyond the natural bone connections. These labeling strategies range from fixed inter-body links to dynamically generated correlations.
- We develop a Two-person Graph Convolution Block (2P-GCB), which enables GCN to learn discriminant spatial-temporal and interactive features simultaneously. To exemplify the effectiveness of 2P-GCB, we test 5 different GCNs by replacing their GCB with our 2P-GCB. For all evaluated GCNs, 2P-GCB obtains higher accuracy than their original GCBs in both individual actions and interactions.
- We propose Two-person Graph Convolutional Network named 2P-GCN. We evaluate our model on the interaction subset of NTU-RGB+D [7], NTU-RGB+D 120 [25], and traditional interaction dataset SBU [5]. Our model achieves state-of-the-art performances on four benchmarks.

II. RELATED WORK

A. Human Interaction Recognition

Human interaction recognition is a sub-topic of action recognition. Most recent action recognition datasets [7], [25]–[27] contain individual actions and multi-person interaction actions.

Most early work [5], [13]–[15] were based on handcrafted features from videos. They often chose a particular descriptor and applied SVM to classify extracted feature vectors. These methods can be divided into local feature approaches, which rely on detecting informative points in the video, and template-based approaches, which consider regions corresponding to a person's body parts [12]. More recent work [16]–[18] usually constructed an end-to-end network to learn features and make classification through CNN and RNN based or combine deep learning techniques with previous methods. RGB videos are sensitive to irrelevant factors like camera motion, background changes, lightness, and occlusions. Therefore, RGB-based methods often require more additional preprocessing and higher computing resources.

Extracted features should be invariant to camera view-points, occlusions, background changes, etc. To improve the robustness, some researchers focused on skeleton data. Yun et al. [5] derived interaction features from the geometric relations among different joints, including intra-body, inter-body, inter-frame, and intra-frame. Then an SVM classifier is utilized for classification. Ji et al. [15] calculated spatial-temporal joint features of 8 interactive body parts (poselets). After removing the redundant information by employing contrast mining, a dictionary is generated based on these features. Finally, an SVM classifier with RBF kernel is adopted for recognition. Alazrai et al. [28] proposed motion-pose geometric descriptors to represent interactions and proved that skeleton pose representation outperforms local space-time features. Wu et al. [29] used sparse-group LASSO to select factors to deal with real-time interaction detection tasks automatically. Perez et al. [10] proposed a relational reasoning network to learn from spatial coordinates of pair-wise joints and perform classification based on inferred relations. Except for the body part to which each joint belongs, this model does not need to know extra prior information, such as the joint label, so it can be easily generalized to multi-person scenarios.

Existing interaction recognition methods are often weak in effectively modeling spatial relationships, motion patterns, and interactive features within a single network. Therefore they cannot obtain competitive results on large-scale interaction datasets.

B. GCN-based methods for interaction recognition

Spatial-based GCN models [19], [21], [22], [24] have been the predominant approaches in skeleton-based action recognition. Most GCNs follow the feature aggregation rule [30] and the graph convolution criteria [9]. When dealing with interaction actions, Conventional GCN-based models consider only one key skeleton or split two persons' skeletons into two separate ones.

Several GCN-based methods tried to model the interactive features [23], [31], [32]. Yang et al. [31] introduced pairwise graph structure by manually adding inter-body links to the isolated two-person graph. Then, they extended ST-GCN to ST-GCN-PAM, which adopts pairwise graph convolution to learn the interactive relation between two persons. Li et al. [32] proposed K-GCN, which introduced a shared knowledge-given graph and dynamically inferred knowledge-learned graph to capture the relations between inter-body joints explicitly. These two graphs and the naturally connected graph controlled three parallel branches in the SGC block. Zhu et al. [23] adopted GCN with separate graphs but especially modeled the interactive feature. They proposed dyadic graph convolution with relational adjacency matrix to capture interaction through a dynamic relational graph and conduct the relational graph convolution as the parallel operation of inter-body graph convolution. They then combined with AGCN [19] and proposed 2S-DRAGCN. 2S-DRAGCN obtains state-of-the-art results on three datasets.

Unlike most GCN-based approaches, K-GCN and 2S-DRAGCN perform inter-body and intra-body graph convolution separately. Their networks can learn interactive information explicitly, whereas they are still in the manner of single-person graph convolution. Therefore, the pairwise graph convolution leads to a complex structure and weak scalability. ST-GCN-PAM is still based on the fixed graph structure and adopts the vanilla ST-GCN backbone, which does not obtain competitive accuracy. In contrast, our model is introduced as a two-person adaptive Graph Convolutional Network. Compared with the aforementioned GCNs, our model with the two-person graph representation has a simpler structure, higher performance, and better generality.

III. METHOD

A. Two-person graph

Previous work put many efforts into modeling the structure of single-person skeleton graphs, ranging from fixed structures [9], [20], [21] to dynamically generated topologies [19], [22], [33]. However, they rarely consider explicitly modeling the relations of inter-body joints. In this section, we will introduce the proposed two-person graph and its corresponding adjacency matrix.

Suppose we use N joints and several bones to construct the skeleton of one person's body. In this way, an interaction sequence performed by two individuals can be represented as a spatio-temporal graph $\mathcal{G} = (\mathcal{V}, \mathcal{E}, \mathcal{X})$, where $\mathcal{V} = \{v_{ti} | t = 1, \dots, T, i = 1, \dots, 2N\}$ is the vertex set of $2N$ joints for two persons in T frames, and \mathcal{E} is the edge set composed of two subsets \mathcal{E}_S and \mathcal{E}_F . \mathcal{E}_F is the temporal connections between each joint and itself in the consecutive frames. In this work, we only consider the modeling of \mathcal{E}_S , which reflects the intra-body and inter-body connection at each frame. $e_{ij} \in \mathcal{E}_S$ represents an undirected edge between v_i and v_j . The adjacency matrix denotes all the edges $\mathbf{A} \in \mathbb{R}^{2N \times 2N}$ and its element a_{ij} stands for the connection strength of e_{ij} . $\mathcal{X} \in \mathbb{R}^{C \times T \times 2N}$ is the feature map of an interaction sequence. This representation can be easily extended to multi-person and human-object interaction scenarios.

a) Three types of connections: As shown in Fig. 1, we classify the edges of a two-person spatial graph into three types. (1) Fixed structure is the natural connections (bones) between skeleton joints. We add one edge between the two body's torsos to ensure that the physical graph is connected. (2) Intra-body connections, including the link between joint pairs which are far away in the fixed structure but have a high correlation. (3) Inter-body connections, which link joints from two different bodies. These connections enable us to define the relationship of interactive joints explicitly. Many previous GCN-based methods attempt to model the intra-body correlation. However, they lack the modeling of inter-body connections, which might be discriminative interactive information for recognizing human-human interactions. In practice, these three types of edges are integrated to form a two-person graph. Note that the strategy for labeling these edges can be arbitrarily defined, and the labeling algorithm can dramatically influence the model performance in our experiments. To exemplify the effect of the two-person graph representation, we explore several labeling strategies, including static and dynamic approaches, in the following section III-B.

B. Edge labeling strategies

As we mentioned in Section III-A, graph edge labeling defines all the edges in the skeleton graph and is crucial for action classification. We present five labeling strategies based on the two-person graph structure, two of which denote static graph while the others are dynamic methods.

As we mentioned in Section III-A, graph edge labeling defines all the edges in the skeleton graph and is crucial for action classification. We present five labeling strategies based on the two-person graph structure, two of which denote static graphs while the others are dynamic methods.

a) Skeleton: Skeleton labeling reflects the natural connection of the human body. For the two-person graph, skeleton labeling includes natural links between joints and one edge between two persons' centers to connect the isolated two skeletons. This strategy is the baseline labeling of our two-person graph. In practice, all the following labeling strategies are implemented with the combination of the fixed skeleton graph. Let \mathbf{A} denote the adjacency matrix of the skeleton graph, and \mathbf{A}^{res} be the relational adjacency matrix defined by one labeling strategy. We replace \mathbf{A} by $\mathbf{A} + \mathbf{A}^{res}$ as a refinement of the graph topology.

b) Pairwise labeling: Yang et al. [31] first developed pairwise links with a two-person graph. This labeling strategy links every corresponding joint among the two-person skeletons. With pairwise links, the GCN model can explicitly extract interactive correlations between joint pairs. In our experiments, the graph with only pairwise links and its combination with the fixed skeleton graph are both examined.

c) Interactive labeling: Different from Pairwise labeling, interactive labeling only connects joints that are considered to have more interaction probability. For example, the edges between both hands of each person and the connections between one person's hand to the other's are constructed. Compared with Pairwise labeling, this labeling strategy could

be more effective as it satisfies graph sparsity by filtering out insignificance correlations.

d) *Geometric labeling*: The above labeling strategies are constructing a fixed graph based on our prior knowledge. In contrast, most current GCNs [22], [33] adopt a dynamically learned graph topology during inference and gain higher performance than fixed graph-based methods. For mutual actions, the interaction features vary dramatically over time. Therefore, inspired by [23], we design a simple but effective metric: spatial relationship, which defines the edge strength by the distance of joints in the Euclidean space. The correlation between two joints is calculated as

$$\delta(x_i, x_j) = \begin{cases} \frac{1}{T} \sum_t \exp(-\frac{\|x_i^t - x_j^t\|^2}{C}) & \text{if } i \neq j \\ 0 & \text{otherwise} \end{cases} \quad (1)$$

In Eq. 1, $x_i^t \in \mathbb{R}^C$ is the coordinate of x_i^t . Based on the distance metric, \mathbf{A}^{res} is defined as

$$\begin{aligned} \mathbf{A}_1^{res}(i, j) &= \widetilde{\mathbf{A}}_1^{-\frac{1}{2}} \delta(x_i, x_j) \widetilde{\mathbf{A}}_1^{-\frac{1}{2}} \quad i, j = 1, \dots, 2N \\ \mathbf{A}_2^{res}(i, j) &= \begin{cases} \widetilde{\mathbf{A}}_2^{-\frac{1}{2}} \delta(x_i, x_j) \widetilde{\mathbf{A}}_2^{-\frac{1}{2}} & i = 1, \dots, N; j = N + 1, \dots, 2N \\ \widetilde{\mathbf{A}}_2^{-\frac{1}{2}} \delta(x_i, x_j) \widetilde{\mathbf{A}}_2^{-\frac{1}{2}} & i = N + 1, \dots, 2N; j = 1, \dots, N \end{cases} \end{aligned} \quad (2)$$

In Eq. 2, \mathbf{A}_0^{res} is set to all zeros. \mathbf{A}_1^{res} denotes joints that are close at the global level, while \mathbf{A}_2^{res} is specialized to capture the inter-body relations. In our experiment, \mathbf{A} is implemented with $\mathbf{A}_d \in \mathbb{R}^{K \times 2N \times 2N}$, $d = 0, 1, 2$ depicts the relations with a graph distance d . Therefore \mathbf{A}^{res} is designed as a geometrical graph topology refinement due to the idea that body contact can imply rich interactive information.

e) *Dynamic labelings*: The above labeling strategies are all manually designed so they may not be suitable for all datasets and models. Recent GCN-based methods have proposed some modules to learn the graph topology dynamically during the training phase. We introduce two adaptive labeling strategies: (1) adaptive adjacency matrix, in which \mathbf{A} is defined as a variable parameter. (2) CTRGC [22]. The authors propose a channel-wise topology refinement module CTRGC to operate graph convolution and generate graph topology for each channel.

We briefly visualize these labeling strategies in Fig. 2. In our experiments, we will examine the proposed edge labeling strategies with our two-person graph.

C. 2P-GCN

The SGC operation is defined as

$$\mathbf{f}_{out} = \sum_j \mathbf{A}_j^{-\frac{1}{2}} (\mathbf{A}_j + \mathbf{A}_j^{res}) \mathbf{A}_j^{-\frac{1}{2}} \mathbf{f}_{in} \mathbf{W}_j, \quad (3)$$

where \mathbf{f}_{in} and \mathbf{f}_{out} are the input and output feature maps. \mathbf{A}_j denotes edges which satisfy the j -th partition strategy. \mathbf{A}_j^{res} is defined by one graph labeling strategy as we discussed in III-B. \mathbf{A}_j is introduced to normalize \mathbf{A}_j , and learnable parameter \mathbf{M}_j is denoted as edge importance weighting.

In [9], the maximum graph sampling distance D is set to 1. We increase D to 2 as the graph size grows and adopt the distance partitioning strategy, which lets \mathbf{A}_j denote the correlation of joints with a graph distance j . In temporal domain, an $L \times 1$ temporal convolution (TCN) is performed

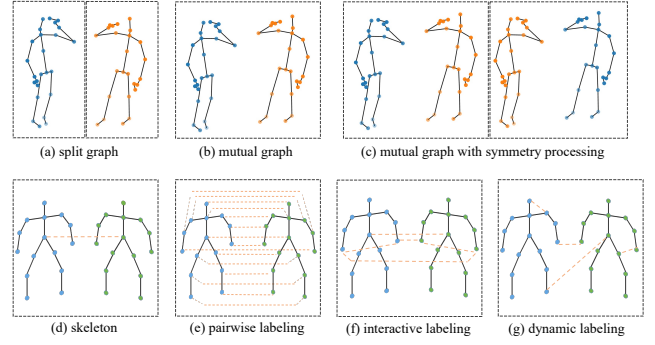


Fig. 2. A brief visualization of different graph structures and edge labeling strategies. The first row (a)-(c) are graph structures that decide the number of joint nodes and samples of a skeleton graph. The first person is in blue while the second person is in orange. The second row (d)-(g) are labeling strategies, which depict different edge labeling strategies over the two-person graph.

on $\mathcal{X} \in \mathbb{R}^{C \times T \times 2N}$ to extract motion features in consecutive frames. SGC and TCN layers are followed by a BatchNorm layer and a ReLU layer, with a block-residual link. SGC, TCN, and an attention layer form a basic block, as illustrated in the top-right corner of Fig.III-C.

Based on 2P-GC, we build a two-person graph convolutional network named 2P-GCN for interaction recognition. Current start-of-the-art methods usually apply multi-stream architecture, consisting of several same GCN streams to process different input data (e.g., joints, bones, motions) and fuse the prediction score at the last FC layer. The multi-modality fusion is proved to be an effective way to enhance the model performance [19], [22], [23]. However, the complexity of the model grows linearly with the addition of branches. Therefore a multi-stream model means a more significant amount of parameters and higher computation cost. Owing to this, inspired by [21], we construct four input branches (joint, bone, joint motion, bone motion as in Figure 3), each of which contains a few blocks respectively. Then we fuse them in the middle of the network. With this architecture, our model can keep the rich information from different inputs and has significantly lower complexity than SOTA methods.

As shown in Fig.3, we adopt the Part-wise Attention Block as in [21], which groups the human skeleton into five functional parts and utilizes Attention mechanism to decide the importance of each part. Previously, the same parts from the two persons are divided into the same group. This body partitioning strategy may not find the crucial part from two persons' skeletons. To this end, we divide two persons into ten parts instead. Our Two-person Graph Convolutional Network can extract and accumulate spatio-temporal and interactive features simultaneously. The entire architecture of our 2P-GCN is illustrated in Fig.3.

D. Good practices for data pre-processing

Many high-performance methods in regular action recognition [19], [22], [24] transform original skeleton data into various forms and feed them into a multi-stream network. We follow these pre-processing idea [21], [24] and create four

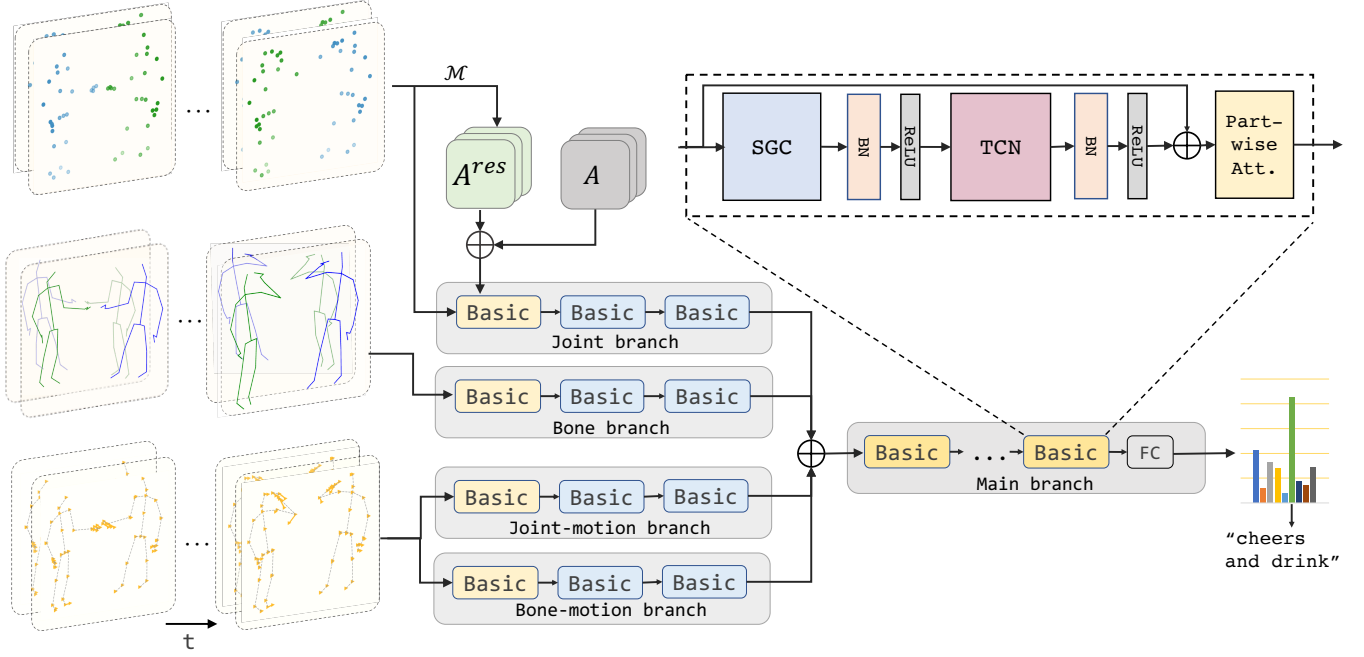


Fig. 3. Illustration of the entire network and detailed structure of the Basic block. From top to the bottom, the 4 input branches are joint, bone, joint motion and bone motion respectively. \mathcal{M} is the graph labeling strategy as discussed in Section III-B. \mathbf{A} denotes the fixed skeleton adjacency matrix, and \mathbf{A}^{res} is the relational adjacency matrix defined by one typical labeling strategy.

input features: joint data, bone data, joint-motion and bone-motion for our model. Let C be the dimension of the joint correlations, the input feature of each joint is represented as a $2C$ -dimensional vector.

a) *Joint*: An action sequence, i.e., a sample in the dataset, is represented as $x \in \mathbb{R}^{C \times T \times 2N}$, where C represents the number of coordinate dimensions. Let x_i^t denote the C -dimensional coordinate of the i -th joint at frame t . The relative position of each joint to the center point (c_0 -th joint) can be calculated as $\bar{x}_i^t = x_i^t - x_{c_0}^t, i = [1, 2, \dots, 2N], t = [1, 2, \dots, T]$. Then the joint input is constructed by concatenating x and \bar{x} to obtain a $2C \times T \times 2N$ -dimensional tensor.

b) *Bone*: The length of the bone feature vector is equal to the number of joints. The bone vector \mathbf{l} and angles between intersecting bones Θ form the bone features. $\mathbf{l}_i = x_i - x_{i_{adj}}, i_{adj} = [1, \dots, T]$, where $x_{i_{adj}}$ is the centripetal adjacent joint of the i -th joint. And the angle of each bone is computed by $\mathbf{a}_{i,k}^t = \arccos(\frac{\mathbf{l}_{i,k}^t}{\|\mathbf{l}_i^t\|_2})$, where $k \in \{1, \dots, C\}$ denotes the k -th dimension (e.g., $\{x, y, z\}$ for 3D skeletons).

c) *Joint motion and bone motion*: The joint-motion inputs are the stack of $\mathbf{v} \in \mathbb{R}^{C \times T \times 2V}$ and $\mathbf{a} \in \mathbb{R}^{C \times T \times 2V}$. The joint motion vector is calculated as

$$\begin{aligned} \mathbf{v}_{\text{joint}}^t &= x^{t+1} - x^t, t = [1, \dots, T-1] \\ \mathbf{a}_{\text{joint}}^t &= x^{t+2} - x^t, t = [1, \dots, T-2] \end{aligned} \quad (4)$$

Similarly, the bone motion vector is computed by

$$\begin{aligned} \mathbf{v}_{\text{bone}}^t &= \mathbf{l}^{t+1} - \mathbf{l}^t, t = [1, \dots, T-1] \\ \mathbf{a}_{\text{bone}}^t &= \mathbf{l}^{t+2} - \mathbf{l}^t, t = [1, \dots, T-2] \end{aligned} \quad (5)$$

To summarize, we first feed the four input feature maps into four input branches. Then we concatenate output features of

all the four branches at an early stage in our network and apply one main branch to learn accumulated features.

d) *Symmetry processing*: We notice that a number of interaction actions are not symmetric. For instance, shaking hands can be considered an interchangeable action, but kicking is not symmetrical, as there are always one subject and one object. During our experiments, we found that adopting the two-person graph may cause accuracy decrease in some actions due to the high intra-class variation caused by the asymmetry. In order to eliminate this variation, we create a reflected sequence by swapping two person's joint labels for each sample. For example, a sequence 'A is kicking B' is replaced by itself and a reflected sequence 'B is kicking A'. After that, these two sequences are stacked along the sample level when feeding into the network. We name this operation symmetry processing, briefly explained in Figure 2-(c).

IV. EXPERIMENTS

A. Datasets

a) *SBU Kinect Interactions*: [5] is a two-person interaction recognition dataset created using Kinect(V1), containing 8 human-human interaction actions (approaching, departing, pushing, kicking, punching, exchanging objects, hugging, and shaking hands). SBU consists of 282 short videos, lasting 2-3 seconds each, involving seven different participants pairing up to 21 permutations. At each frame, 3D coordinates over 15 skeleton joints for each candidate are provided. For evaluation, we follow the 5-fold cross validation defined by the authors and report the average accuracy.

b) *NTU-RGB+D*: [7] is not specifically for interaction recognition. NTU dataset was released in 2016, including more than 56,000 action sequences, covering 60 action categories (11 of them are human-human interaction actions). All the skeleton data are recorded by three Kinect v2 cameras from different viewpoints. For the 3D skeleton data, 3D coordinates of 25 joints of each person were collected in each frame. In this paper, for regular skeleton action recognition, the entire NTU dataset is used. While for interaction recognition, we only use the mutual action subset, denoted as NTU-mutual, which is notwithstanding the largest skeleton interaction dataset up to now.

NTU-mutual contains a total of 10,347 samples performing by 40 subjects. In each frame, 3D coordinates of 50 skeleton joints (25 for each person) are given. There are two widely-used benchmarks developed by the authors: (1) **Cross-subject (X-sub)** divides samples into training set (7,319 samples) and testing set (3,028 samples) by splitting 40 volunteers into two groups. (2) **Cross-view (X-view)** benchmark takes the camera ID as division basis, in which samples taken by camera 2 and 3 are used for training (6,889 samples), while samples collected by camera 1 are reserved for testing (3,458 samples).

c) *NTU-RGB+D 120*: [25] is the extended version of NTU-RGB+D. NTU120 expands NTU-RGB+D by adding another 57,367 samples over 60 novel action classes (26 of the 120 classes are labeled as mutual action). We likewise extract the mutual action subset denoted as **NTU120-mutual** for interaction recognition. The authors also provide two recommended benchmarks: **cross subject (X-sub120)** and **cross setup (X-set120)**. The cross setup benchmark splits by camera configurations (the distance and height of the camera to the subject relatively), taking 13,072 samples as training set and remaining 11,660 samples as test set. The cross subject benchmark contains 11,864 samples for training and 12,868 samples for testing.

B. Implementation details

a) *Pre-processing*: As we discussed in section III-D, the input features are represented as $\mathbf{f}_{in} \in \mathbb{R}^{C \times T \times 2N}$, where $C = 6$ for 3D skeleton data. We set $T = 300$ for NTU-RGB+D and 100 for SBU. The sequences with less than T frames are padded by blank frames at the end.

b) *Model configurations*: In the setting of convolutional window size, we follow [21]. The temporal convolution window L is set to 9 and the maximum graph sampling length D is set to 2. The batch size of training set and test set is 16. We train our model for 50 epochs and use a warm-up strategy [34] at the first 5 epochs. We choose Cross-Entropy as the loss function, adopt an SGD optimizer with the Nesterov momentum of 0.9 and the weight decay of 0.0002. The learning rate is initialized to 0.1. All the experiments are conducted on one NVIDIA GeForce RTX 3090 GPU.

C. Ablation study for interaction recognition

a) *Graph structure*: We first evaluate the effectiveness of our two-person graph in interaction recognition. For the first ablation study, we compare the recognition accuracy of

TABLE I
ABLATION STUDY FOR DIFFERENT GRAPH STRUCTURES AND LABELING STRATEGIES. FOR $\text{SHAPE}(N, M)$, N IS THE NUMBER OF JOINTS IN A GRAPH (FOR NTU DATASET $N = 25$ EACH PERSON), M IS THE NUMBER OF GRAPHS CREATED FOR EACH SAMPLE. WE TEST ALL 5 LABELING STRATEGIES IN SECTION III-B WITH THE MUTUAL GRAPH STRUCTURE. FOR $\text{KERNEL}(L, K)$, L IS THE TEMPORAL WINDOW SIZE FOR TCN, AND $K = D + 1$ IS THE NUMBER OF SUBSET OF ADJACENCY MATRIX \mathbf{A} . K IS DEFINED BY THE DISTANCE PARTITION STRATEGY, IN WHICH \mathbf{A}_j DENOTE THE CORRELATION OF JOINTS WITH A GRAPH DISTANCE j .

| Graph structure | Shape(N, M) | X-Sub120 \pm Std. | X-Set120 \pm Std. |
|-----------------|-----------------|----------------------------------|----------------------------------|
| Baseline | (25,2) | 90.48 \pm 0.05 | 90.50 \pm 0.13 |
| Mutual | (50,1) | 91.52 \pm 0.20 | 91.58 \pm 0.13 |
| Zero-padding | (50,2) | 91.66 \pm 0.05 | 91.56 \pm 0.17 |
| Symmetry | (50,2) | 92.24\pm0.09 | 92.50\pm0.02 |

| Labeling strategy | Kernel(L, K) | X-Sub120 | X-Set120 |
|--------------------------|------------------|--------------|--------------|
| Fully connected | (9,1) | 85.33 | 87.51 |
| Only pairwise link | (9,1) | 90.56 | 90.58 |
| Pairwise labeling | (9,2) | 90.66 | 90.61 |
| Pairwise labeling | (9,3) | 90.93 | 90.94 |
| Skeleton(Only self link) | (9,1) | 90.45 | 90.45 |
| Skeleton | (9,2) | 91.30 | 91.50 |
| Skeleton(Baseline) | (9,3) | 91.52 | 91.58 |
| Interactive labeling | (9,3) | 91.28 | 91.14 |
| Geometric labeling | (9,3) | 91.69 | 91.26 |
| Adaptive \mathbf{A} | (9,3) | 89.67 | 90.05 |
| CTRGC [22] | (9,3) | 91.25 | 92.05 |

four graph structure configurations: (1) Baseline (split graph): The input two-person features are structured as two separated graphs, as most GCNs adopted; (2) Mutual: Two-person graph is adopted; (3) Symmetry: This configuration enhances the input data by adding a reflected sequence for each sample as the second sample. (4) Padding: The control group of symmetry processing. This config creates an all-zero mirror for each sample. Config (1) is with the single-person graph, while config (2)-(4) are based on the two-person graph with different processing techniques. Except for the number of nodes in the graph, all 4 graphs adopt Skeleton labeling. We present the recognition accuracy of these graph structures in the top rows of Table I, where we have the following observations: (1) With our two-person graph, the recognition accuracy is significantly improved by over 1% than baseline. This result proves that our two-person graph has the advantage of the existing single-person graph representation. (2) Symmetry processing outperforms naive two-person graphs on all benchmarks. This result shows that symmetry processing can significantly improve the performance of interaction classification under two-person graph-based models.

b) *Graph labeling strategy*: Yan et al. [9] first introduced GCN in skeleton action recognition and evaluated the performance of ST-GCN with three presented graph partition strategies. However, no one has done similar experiments on a two-person graph before. Owing to this, we compare our model's accuracy under different graph labeling strategies, as shown in Table I. We have the following observations: (1) A fully connected graph obtains the lowest accuracy, which indicates that graph sparsity is essential for classification. (2) For Pairwise labeling and Skeleton labeling, partitioning with more subsets is generally better than with fewer subsets. This proves the effectiveness of increasing maximum graph sampling distance D to 2 as a two-person graph has double

TABLE II

COMPARISONS OF ACCURACY (%) FOR ABLATION STUDY OF THE TWO-PERSON GRAPH REPRESENTATION. WE TEST SEVERAL GCNs WITH THEIR ORIGINAL GRAPH STRUCTURE AND OUR TWO-PERSON SKELETON GRAPH (WITH *mutual* SUFFIX) ON NTU-MUTUAL AND NTU120-MUTUAL.

| GCN | NTU-mutual | | NTU120-mutual | |
|-------------------------------|--------------|--------------|---------------|--------------|
| | X-Sub | X-View | X-Sub120 | X-Set120 |
| ST-GCN [9] | 89.31 | 93.72 | 80.69 | 80.27 |
| ST-GCN mutual | 91.05 | 94.58 | 83.39 | 82.46 |
| 2S-AGCN [19] | 93.36 | 96.67 | 87.83 | 89.21 |
| 2S-AGCN mutual | 93.96 | 97.22 | 87.93 | 89.69 |
| ResGCN [21] | 94.34 | 97.55 | 89.64 | 89.94 |
| ResGCN mutual | 95.69 | 98.27 | 91.27 | 91.90 |
| CTR-GCN [22] | 96.33 | 98.75 | 92.03 | 92.82 |
| CTR-GCN mutual | 96.76 | 98.87 | 92.26 | 92.91 |
| EfficientGCN-B4 [35] | 96.00 | 98.35 | 90.8 | 90.75 |
| EfficientGCN-B4 mutual | 95.87 | 98.73 | 91.90 | 92.46 |

TABLE III

COMPARISON WITH DIFFERENT INPUT FEATURES ON NTU-MUTUAL CROSS-SUB (X-SUB) AND NTU120-MUTUAL CROSS-SUB (X-SUB120) IN ACCURACY (%) FOR ABLATION STUDY. J=JOINTS, B=BONES, JM=JOINT MOTIONS, BM=BONE MOTIONS.

| Input data | NTU120-mutual | |
|------------------------|-------------------|-------------------|
| | X-Sub120 | X-Set120 |
| BM | 86.56±0.20 | 87.04±0.31 |
| B | 88.22±0.13 | 89.14±0.07 |
| JM | 88.55±0.20 | 88.80±0.30 |
| J | 90.09±0.04 | 90.64±0.17 |
| J + B | 91.18±0.04 | 91.09±0.16 |
| J + B + JM | 92.24±0.08 | 92.50±0.02 |
| J + B + JM + BM | 92.38±0.03 | 92.62±0.01 |

nodes than before. (3) Compared with Pairwise labeling, Interactive labeling obtains higher performance but is still lower than Skeleton labeling. These results demonstrate that manually adding inter-body edges may not benefit our model in identifying interactions. (4) For Adaptive labelings, letting adjacency matrix \mathbf{A} be adaptive makes no improvement, which proves that simply adopting dynamic topology in a two-person graph does not work as the single-person scenario. (5) The results of Geometric labeling and CTRGC show that our model can effectively integrate intra-body and interactive information with a carefully designed adaptive labeling strategy.

c) Two-person graph convolution block: To examine the effectiveness of the proposed two-person graph representation for convincing results, we evaluate several GCN models with our two-person graph setup. For each GCN, we only modify the structure of the *fixed* graph to our two-person graph and keep other parameters unchanged. The classification accuracy of these GCNs is shown in Table II, from which almost all these GCNs with the two-person graph are stably better than the original ones. This phenomenon further confirms the effectiveness and generalizability of adopting a two-person graph in interaction recognition.

d) Multi-branch Input data: Most of the current high-performance models apply multi-stream GCNs with different input data, and these models suffer from high computational costs and several times more parameters. We integrate the idea of [21], [24] and fuse the four input branches (joint, bone,

TABLE IV

COMPARISONS OF ACCURACY (%) ON NTU-RGB+D AND NTU-RGB+D 120 FOR ABLATION STUDY. WE TEST ST-GCN AND RESGCN WITH THEIR ORIGINAL GRAPH STRUCTURE AND WITH OUR 2-PERSON SKELETON GRAPH (*mutual* SUFFIX). FOR MUTUAL GRAPH, SYMMETRY PROCESSING IS ADOPTED.

| GCN | NTU-RGB+D | | NTU-RGB+D 120 | |
|-----------------------------|--------------|--------------|---------------|--------------|
| | X-Sub | X-View | X-Sub120 | X-Set120 |
| ST-GCN [9] | 79.90 | 89.82 | 72.95 | 74.99 |
| ST-GCN mutual | 81.65 | 90.96 | 75.41 | 76.15 |
| Pa-ResGCN-B19 [21] | 90.82 | 95.78 | 86.55 | 87.94 |
| Pa-ResGCN-B19 mutual | 91.05 | 95.98 | 86.96 | 88.43 |

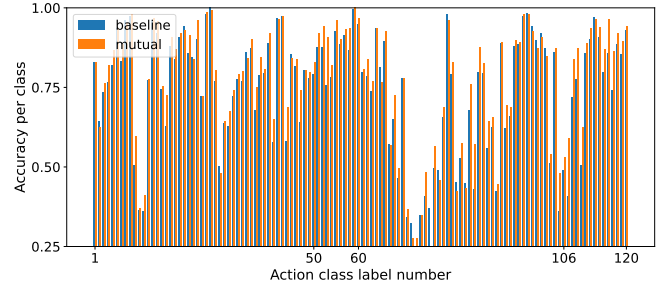


Fig. 4. Accuracy comparison of each action class between ST-GCN baseline and ST-GCN with our 2P-GCB (mutual) on NTU-RGB+D 120 Cross-subject. Our two-person graph outperforms the baseline on most actions, especially for interactions (No.50-60,106-120).

joint motion, bone motion) in the middle of our model instead of the final decision stage. To examine the necessity of each input, we present Table III. All the experiments are performed more than 5 times, and the standard error is provided. In Table III, our model with all four inputs obtains the highest accuracy than others. As the number of features increases, the performance improves steadily. This indicates that all four input data are informative for the interaction recognition tasks, and our model can effectively accumulate crucial information from these inputs.

D. Ablation study for single person action recognition

The idea of two-person graph representation is compatible with single-person inputs. GCN approaches create two samples of skeleton data for each sample and extract features of actions individually. This processing discards the interactive information when dealing with mutual actions. However, our two-person graph structure keeps the interactive information without additional computation cost. We present the model performance of ST-GCN and our 2P-GCN's backbone ResGCN on the NTU-RGB+D dataset, as shown in Table IV. When adopting a two-person graph with symmetry processing, ST-GCN gains significant improvement, and the accuracy of ResGCN still increases. To figure out where 2P-GC outperforms 1P-GC, we compare the F1 scores of STGCN with 2P-GC and its original 1P-GC on the X-sub120 benchmark of NTU120-mutual, as Figure 4 shows. We notice that STGCN with 2P-GC outperforms its baseline on almost all actions. The margin is more significant on interaction actions (no.50-60, 106-120). This is strong proof that the two-person graph representation is an ideal substitution for the single graph.

TABLE V
COMPARISONS OF AVERAGE ACCURACY (%) WITH OTHER SOTA
METHODS ON SBU INTERACTIONS.

| Method | Accuracy |
|--------------------------------------|--------------|
| ST-LSTM [36] | 93.30 |
| IRN _{inter+intra} [10] | 96.10 |
| K-GCN [32] | 97.20 |
| LSTM-IRN _{inter+intra} [10] | 98.20 |
| VA-fusion [37] | 98.30 |
| HCN [38] | 98.60 |
| DR-GCN [23] | 99.06 |
| 2P-GCN (Ours) | 98.90 |

TABLE VI
STATE-OF-THE-ART METHODS COMPARISON IN ACCURACY (%) ON
NTU-MUTUAL DATASET.

| Method | Conference | X-Sub | X-View |
|------------------------------------|-------------|--------------|--------------|
| ST-LSTM* [36] | TPAMI17 | 83.00 | 87.30 |
| GCA-LSTM* [39] | CVPR17 | 85.90 | 89.00 |
| 2S-GCA-LSTM [40] | TIP17 | 87.20 | 89.90 |
| LSTM-IRN [10] | TMM21 | 90.50 | 93.50 |
| DR-GCN [23] | PR21 | 93.68 | 94.09 |
| K-GCN [32] | NEUROCOMP21 | 93.70 | 96.80 |
| 2S-DRAGCN [23] | PR21 | 94.68 | 97.19 |
| ST-GCN [◇] [9] | AAAI18 | 89.31 | 93.72 |
| AS-GCN* [33] | CVPR19 | 89.30 | 93.00 |
| 2S-AGCN [◇] [19] | CVPR19 | 93.36 | 96.67 |
| Pa-ResGCN-B19 [◇] [21] | ACMMM20 | 94.34 | 97.55 |
| CTR-GCN [◇] [22] | CVPR21 | 95.31 | 97.60 |
| EfficientGCN-B4 [◇] [35] | TPAMI22 | 96.00 | 98.35 |
| 2P-GCN w/ fixed graph (Ours) | - | 96.06 | 98.94 |
| 2P-GCN w/ distance labeling (Ours) | - | 96.40 | 98.50 |
| 2P-GCN w/ CTRGC (Ours) | - | 97.03 | 99.05 |

* Results are reported in [10]

◇ Results are produced by us with author-published codes.

E. Comparison with the SOTA methods

a) *SBU*: We compare the average accuracy of our best results on the 5-fold cross-validation with state-of-the-art results on SBU. As shown in Table V, our model obtains an accuracy close to SOTA methods. Note that SBU is a dataset containing only 282 samples. This experiment shows that our model can achieve promising results even on a small dataset.

b) *NTU-mutual and NTU120-mutual*: We compare our network with two types of models. The first group consists of the predominant methods in interaction recognition. Most of them are hand-crafted or LSTM based methods, including ST-LSTM [36], GCA-LSTM [39], 2S-GCA-LSTM [40], LSTM-IRN [10], ST-GCN-PAM [31], K-GCN [32], DR-GCN and 2S-DRAGCN [23]. The second group is regular GCN-based networks, which separate two-person graph into two separate skeletons, including ST-GCN [9], AS-GCN [33], 2S-AGCN [19], Pa-ResGCN-B19 [21], EfficientGCN-B4 [35], CTR-GCN [22]. We make these results on NTU-mutual with their published code. As shown in Table VI and Table VII, our model with the fixed two-person graph outperforms current state-of-the-art 2S-DRGCN [23] by 1.38%, 1.34%, 1.82% and 2.19% on 4 benchmarks respectively. Moreover, 2P-GCN with geometric graph labeling obtains a higher performance than the fixed graph on three benchmarks, which shows our model can effectively capture the interaction information among inter-body contacts. Finally, 2P-GCN with CTRGC obtains higher performance than other models, constructing a signif-

TABLE VII
STATE-OF-THE-ART METHODS COMPARISON IN ACCURACY (%) ON
NTU120-MUTUAL DATASET.

| Method | Conference | X-Sub120 | X-Set120 |
|------------------------------------|------------|--------------|--------------|
| ST-LSTM* [36] | TPAMI17 | 63.00 | 66.60 |
| GCA-LSTM* [39] | CVPR17 | 70.60 | 73.70 |
| 2S-GCA-LSTM* [40] | TIP17 | 73.00 | 73.30 |
| LSTM-IRN [10] | TMM21 | 77.70 | 79.60 |
| ST-GCN-PAM [31] | ICIP20 | 83.28 | 88.36 |
| DR-GCN [23] | PR21 | 85.36 | 84.49 |
| 2S-DRAGCN [23] | PR21 | 90.56 | 90.43 |
| ST-GCN [◇] [9] | AAAI18 | 80.69 | 80.27 |
| AS-GCN* [33] | CVPR19 | 82.90 | 83.70 |
| 2S-AGCN [◇] [19] | CVPR19 | 87.83 | 89.21 |
| Pa-ResGCN-B19 [◇] [21] | ACMMM20 | 89.64 | 89.94 |
| CTR-GCN [◇] [22] | CVPR21 | 92.03 | 92.82 |
| EfficientGCN-B4 [◇] [35] | TPAMI22 | 90.80 | 90.75 |
| 2P-GCN w/ fixed graph (Ours) | - | 92.38 | 92.62 |
| 2P-GCN w/ distance labeling (Ours) | - | 92.70 | 92.27 |
| 2P-GCN w/ CTRGC (Ours) | - | 92.36 | 93.24 |

* Results are reported in [10]

◇ Results are produced by us with author-published codes.

icantly higher baseline in the skeleton interaction recognition task.

V. CONCLUSION

In this work, we proposed an adaptive two-person Graph Convolutional Network named 2P-GCN. First, we introduced the two-person graph as a substitution for the isolated single-person graph to represent human-human interactions. Next, we built a two-person Spatial Graph Convolution Layer, which can learn predominant features from intra-body and inter-body interactions. When adopting our two-person graph topology, experiments showed significant accuracy improvement in both single-person and interaction actions. Finally, results on three datasets show that our proposed 2P-GCN obtains state-of-the-art performances. In the future, we will extend the proposed two-person graph to human-object interaction and group activity recognition, and attempt to construct a generic representation of human actions.

ACKNOWLEDGMENTS

This work was supported by the Guangdong Basic and Applied Basic Research Foundation under Grant 2022A1515010800.

REFERENCES

- [1] Y. Ji, Y. Yang, F. Shen, H. T. Shen, and X. Li, "A survey of human action analysis in hri applications," *IEEE Trans. Circuits Syst. Video Technol.*, vol. 30, no. 7, pp. 2114–2128, 2020.
- [2] Z. Zhang, "Microsoft kinect sensor and its effect," *IEEE Multimedia*, vol. 19, no. 2, pp. 4–10, 2012.
- [3] Z. Cao, G. Hidalgo, T. Simon, S.-E. Wei, and Y. Sheikh, "Openpose: realtime multi-person 2d pose estimation using part affinity fields," *IEEE Trans. Pattern Anal. Mach. Intell.*, vol. 43, no. 1, pp. 172–186, 2019.
- [4] K. Sun, B. Xiao, D. Liu, and J. Wang, "Deep high-resolution representation learning for human pose estimation," in *IEEE Conf. Comput. Vis. Pattern Recognit. (CVPR)*, 2019, pp. 5693–5703.
- [5] K. Yun, J. Honorio, D. Chattopadhyay, T. L. Berg, and D. Samaras, "Two-person interaction detection using body-pose features and multiple instance learning," in *IEEE Conf. Comput. Vis. Pattern Recognit. Workshops (CVPRW)*. IEEE, 2012, pp. 28–35.
- [6] R. Vemulapalli, F. Arrate, and R. Chellappa, "Human action recognition by representing 3d skeletons as points in a lie group," in *IEEE Conf. Comput. Vis. Pattern Recognit. (CVPR)*, 2014, pp. 588–595.

- [7] A. Shahroudy, J. Liu, T.-T. Ng, and G. Wang, "Ntu rgb+ d: A large scale dataset for 3d human activity analysis," in *IEEE Conf. Comput. Vis. Pattern Recognit. (CVPR)*, 2016, pp. 1010–1019.
- [8] Y. Hou, Z. Li, P. Wang, and W. Li, "Skeleton optical spectra-based action recognition using convolutional neural networks," *IEEE Trans. Circuits Syst. Video Technol.*, vol. 28, no. 3, pp. 807–811, 2018.
- [9] S. Yan, Y. Xiong, and D. Lin, "Spatial temporal graph convolutional networks for skeleton-based action recognition," in *AAAI Conf. Artif. Intell.*, 2018, pp. 7444–7452.
- [10] M. Perez, J. Liu, and A. C. Kot, "Interaction relational network for mutual action recognition," *IEEE Trans. Multimedia*, 2021.
- [11] P. Khaire and P. Kumar, "Deep learning and rgb-d based human action, human–human and human–object interaction recognition: A survey," *J. Vis. Commun. Image R.*, vol. 86, p. 103531, 2022.
- [12] A. Stergiou and R. Poppe, "Analyzing human–human interactions: A survey," *Comput. Vis. Image Underst.*, vol. 188, p. 102799, 2019.
- [13] Y. Zhang, X. Liu, M.-C. Chang, W. Ge, and T. Chen, "Spatio-temporal phrases for activity recognition," in *Eur. Conf. Comput. Vis. (ECCV)*. Springer, 2012, pp. 707–721.
- [14] Y. Kong, Y. Jia, and Y. Fu, "Learning human interaction by interactive phrases," in *Eur. Conf. Comput. Vis. (ECCV)*. Springer, 2012, pp. 300–313.
- [15] Y. Ji, G. Ye, and H. Cheng, "Interactive body part contrast mining for human interaction recognition," in *IEEE Int. Conf. Multimedia Expo Workshop (ICMEW)*. IEEE, 2014, pp. 1–6.
- [16] J. Donahue, L. Anne Hendricks, S. Guadarrama, M. Rohrbach, S. Venugopalan, K. Saenko, and T. Darrell, "Long-term recurrent convolutional networks for visual recognition and description," in *IEEE Conf. Comput. Vis. Pattern Recognit. (CVPR)*, 2015, pp. 2625–2634.
- [17] M. Sadegh Aliakbarian, F. Sadat Saleh, M. Salzmann, B. Fernando, L. Petersson, and L. Andersson, "Encouraging lstms to anticipate actions very early," in *IEEE Conf. Comput. Vis. Pattern Recognit. (CVPR)*, 2017, pp. 280–289.
- [18] X. Wang and Q. Ji, "Hierarchical context modeling for video event recognition," *IEEE Trans. Pattern Anal. Mach. Intell.*, vol. 39, no. 9, pp. 1770–1782, 2017.
- [19] L. Shi, Y. Zhang, J. Cheng, and H. Lu, "Two-stream adaptive graph convolutional networks for skeleton-based action recognition," in *IEEE Conf. Comput. Vis. Pattern Recognit. (CVPR)*, 2019, pp. 12 026–12 035.
- [20] Y.-F. Song, Z. Zhang, C. Shan, and L. Wang, "Richly activated graph convolutional network for robust skeleton-based action recognition," *IEEE Trans. Circuits Syst. Video Technol.*, vol. 31, no. 5, pp. 1915–1925, 2021.
- [21] Y.-F. Song, Z. Zhang, C. Shan, and L. Wang, "Stronger, faster and more explainable: A graph convolutional baseline for skeleton-based action recognition," in *ACM Int. Conf. Multimedia (ACMMM)*, 2020, pp. 1625–1633.
- [22] Y. Chen, Z. Zhang, C. Yuan, B. Li, Y. Deng, and W. Hu, "Channel-wise topology refinement graph convolution for skeleton-based action recognition," in *IEEE Int. Conf. Comput. Vis. (ICCV)*, 2021, pp. 13 359–13 368.
- [23] L. Zhu, B. Wan, C. Li, G. Tian, Y. Hou, and K. Yuan, "Dyadic relational graph convolutional networks for skeleton-based human interaction recognition," *Pattern Recognit.*, vol. 115, p. 107920, 2021.
- [24] Z. Liu, H. Zhang, Z. Chen, Z. Wang, and W. Ouyang, "Disentangling and unifying graph convolutions for skeleton-based action recognition," in *IEEE Conf. Comput. Vis. Pattern Recognit. (CVPR)*, 2020, pp. 143–152.
- [25] J. Liu, A. Shahroudy, M. Perez, G. Wang, L.-Y. Duan, and A. C. Kot, "Ntu rgb+ d 120: A large-scale benchmark for 3d human activity understanding," *IEEE Trans. Pattern Anal. Mach. Intell.*, vol. 42, no. 10, pp. 2684–2701, 2019.
- [26] H. Kuehne, H. Jhuang, E. Garrote, T. Poggio, and T. Serre, "Hmdb: a large video database for human motion recognition," in *IEEE Int. Conf. Comput. Vis. (ICCV)*. IEEE, 2011, pp. 2556–2563.
- [27] W. Kay, J. Carreira, K. Simonyan, B. Zhang, C. Hillier, S. Vijayanarasimhan, F. Viola, T. Green, T. Back, P. Natsev *et al.*, "The kinetics human action video dataset," *arXiv preprint arXiv:1705.06950*, 2017.
- [28] R. Alazrai, Y. Mowafi, and C. G. Lee, "Anatomical-plane-based representation for human–human interactions analysis," *Pattern Recognit.*, vol. 48, no. 8, pp. 2346–2363, 2015.
- [29] H. Wu, J. Shao, X. Xu, Y. Ji, F. Shen, and H. T. Shen, "Recognition and detection of two-person interactive actions using automatically selected skeleton features," *IEEE Trans. Human-Mach. Syst.*, vol. 48, no. 3, pp. 304–310, 2017.
- [30] M. Welling and T. N. Kipf, "Semi-supervised classification with graph convolutional networks," in *Proc. Int. Conf. Learn. Represent. (ICLR)*, 2017.
- [31] C.-L. Yang, A. Setyoko, H. Tampubolon, and K.-L. Hua, "Pairwise adjacency matrix on spatial temporal graph convolution network for skeleton-based two-person interaction recognition," in *IEEE Int. Conf. Image Process (ICIP)*. IEEE, 2020.
- [32] J. Li, X. Xie, Y. Cao, Q. Pan, Z. Zhao, and G. Shi, "Knowledge embedded gcn for skeleton-based two-person interaction recognition," *Neurocomputing*, vol. 444, pp. 338–348, 2021.
- [33] M. Li, S. Chen, X. Chen, Y. Zhang, Y. Wang, and Q. Tian, "Actional-structural graph convolutional networks for skeleton-based action recognition," in *IEEE Conf. Comput. Vis. Pattern Recognit. (CVPR)*, 2019, pp. 3595–3603.
- [34] K. He, X. Zhang, S. Ren, and J. Sun, "Deep residual learning for image recognition," in *IEEE Conf. Comput. Vis. Pattern Recognit. (CVPR)*, 2016, pp. 770–778.
- [35] Y.-F. Song, Z. Zhang, C. Shan, and L. Wang, "Constructing stronger and faster baselines for skeleton-based action recognition," *IEEE Trans. Pattern Anal. Mach. Intell.*, pp. 1–1, 2022.
- [36] J. Liu, A. Shahroudy, D. Xu, A. C. Kot, and G. Wang, "Skeleton-based action recognition using spatio-temporal lstm network with trust gates," *IEEE Trans. Pattern Anal. Mach. Intell.*, vol. 40, no. 12, pp. 3007–3021, 2017.
- [37] P. Zhang, C. Lan, J. Xing, W. Zeng, J. Xue, and N. Zheng, "View adaptive neural networks for high performance skeleton-based human action recognition," *IEEE Trans. Pattern Anal. Mach. Intell.*, vol. 41, no. 8, pp. 1963–1978, 2019.
- [38] C. Li, Q. Zhong, D. Xie, and S. Pu, "Co-occurrence feature learning from skeleton data for action recognition and detection with hierarchical aggregation," in *IJCAI Int. Joint Conf. Artif. Intell.*, 2018, pp. 786–792.
- [39] J. Liu, G. Wang, P. Hu, L.-Y. Duan, and A. C. Kot, "Global context-aware attention lstm networks for 3d action recognition," in *IEEE Conf. Comput. Vis. Pattern Recognit. (CVPR)*, 2017, pp. 1647–1656.
- [40] J. Liu, G. Wang, L.-Y. Duan, K. Abdiyeva, and A. C. Kot, "Skeleton-based human action recognition with global context-aware attention lstm networks," *IEEE Trans. Image Process.*, vol. 27, no. 4, pp. 1586–1599, 2017.